Inorganic Chemistry

pubs.acs.org/IC Article

Versatility of Tellurium in Heteroanionic Ln_2O_2Te (Ln = La, Ce, Pr) and Tellurate Ln_2TeO_6 (Ln = La, Pr)

Melissa S. Orr, Katheryn R. Cruz, Hoa H. Nguyen, Akari L. Kojima, and Robin T. Macaluso*

Cite This: *Inorg. Chem.* 2022, 61, 18002−18009 Read Online

ACCESS | Metrics & More | Article Recommendations | Supporting Information

ABSTRACT: Heteroanionic compounds continue to gain interest in materials design because the expanded composition space provides opportunities to discover new phases and tune physical properties. Among heteroanionic materials, oxytellurides comprised of oxygen and tellurium anions are relatively underexplored despite the significant role of tellurium in emerging technologies. Herein, we present synthetic strategies toward oxytelluride Ln_2O_2Te (Ln = La−Pr), whose layered structure features square nets of Te^{2-} anions. Upon heating in H_2 or air, we find a reversible phase transition between the oxytelluride and tellurate Ln_2TeO_6 (Ln = La, Pr), wherein Te is octahedrally coordinated and a 6+ oxidation state is corroborated by bond valence analysis. We use X-ray diffraction along with thermogravimetric analyses to confirm the presence of oxytelluride and tellurate phases and emphasize key structural distinctions. In contrast, we find that Ce_2O_2Te decomposes to form CeO_2 and demonstrate the instability of Ce_2O_2Te in ambient conditions by timelapse X-ray diffraction and diffuse-reflectance spectroscopy experiments. Band gaps of Ln_2O_2Te (Ln = La−Pr) were estimated from diffuse-reflectance spectroscopy in the semiconducting range ~2.1−2.7 eV, while band gaps for La_2TeO_6 and Pr_2TeO_6 were much larger at ~4.3 and ~3.7 eV, respectively.

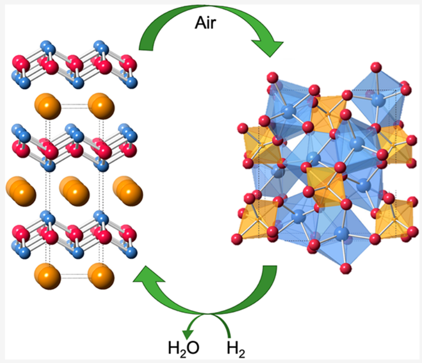

■ INTRODUCTION

Heteroanionic systems have emerged as a distinct class of materials for which exploration of the anion composition presents an exciting opportunity to strategically target new materials and tune physical properties.[1−3] Greater structural diversity afforded by the expanded composition space often results in interesting characteristics otherwise inaccessible through conventional cation substitution or homoanionic systems. As a result of modern computationally driven materials screening techniques, heteroanionic systems are highlighted as promising candidates in advanced applications such as transparent semiconductors, solid-state electrolytes, thermoelectrics, and optoelectronics.[4−7] Work on ternary and quaternary heteroanionic systems like oxysulfides, oxyselenides, oxynitrides, and oxychlorides are well underway; however, relatively few oxytellurides have been reported.[8−11] This lack of attention is perhaps a reflection of the low natural abundance of tellurium and the invalid assumption that structure−property relationships of tellurium compounds can be inferred from those of their lighter chalcogen counterparts.[12]

As an energy-critical element[13] prominent in innovative energy technologies, tellurium is unique from other chalcogens in terms of its structure, properties, and reactivity.[12] Although chalcogenides are known for their broad range of oxidation states, from 2− to 6+, the higher oxidation states are more stable for tellurium because of its lower ionization energy. Te-centered octahedra are unique to tellurates, whereas sulfates and selenates are commonly characterized by tetrahedral coordination of chalcogen, which bonds more tightly with the O atoms.[14] For instance, the three-dimensional framework of solid-state paratellurite (α-TeO_2) is characterized by Te^{4+} in a distorted octahedral coordination and is in marked contrast to the monomeric structure of SO_2, which is a toxic gas.[12]

Oxychalcogenides face some noteworthy synthetic challenges often because of the ease of volatility of chalcogen precursors, therefore requiring controlled atmospheres or alternatives to conventional inorganic synthetic methods. A common protocol for synthesizing oxysulfides, for example, uses H_2S gas as a sulfurizing agent; however, there is no analogous protocol for synthesizing oxytellurides. By comparison, H_2Te gas is highly unstable, rapidly degrading in the presence of air or light, and not commercially available.[15] Herein, we first attempt to better understand the synthesis and characterization of mixed O−Te phases, and to the best of our knowledge, M_2O_2Te ($M = 3^+$ metal) is the only known ternary oxytelluride.

In this paper, we investigate synthetic pathways toward Ln_2O_2Te (Ln = La, Ce, Pr) and demonstrate the reversible transformation of oxytelluride Ln_2O_2Te (Ln = La, Pr) to the

Received: June 30, 2022
Published: November 1, 2022

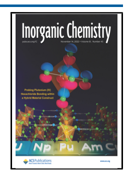

respective tellurates, Ln_2TeO_6. This reversible phase transition from oxytelluride to tellurate showcases the broad range of tellurium oxidation states as well as its unique coordination and reactivity. We find Ce_2O_2Te instead to be air-sensitive and to show gradual degradation. We also present structural and optical measurements that distinguish the oxytellurides from tellurates. These are the first quantitative reports of the physical properties of Ln_2O_2Te (Ln = La, Ce, Pr).

■ EXPERIMENTAL METHODS

Reagents. La rod (99.9%, Alfa Aesar), Ce rod (99.9%, Alfa Aesar), Pr rod (99.9%, Alfa Aesar), La_2O_3 (99.9%, TCI America), CeO_2 (99.9%, Alfa Aesar), Pr_2O_3 (99.9%, Alfa Aesar), α-TeO_2 (99.99%, Alfa Aesar), and Te shot (99.9999%, Alfa Aesar) were used as received without any additional purification for oxytelluride syntheses. La_2O_3 (99.9%, TCI America) and Pr_2O_3 (99.9%, Alfa Aesar) were calcined prior to use in tellurate syntheses.

Ln_2O_2Te Oxytelluride Synthesis. Bulk samples of Ln_2O_2Te (Ln = La, Ce, Pr) were prepared by two different synthetic methods, which are categorized hereafter according to the furnace used for heating, either a muffle furnace or a tube furnace. The muffle furnace method follows a standard solid-state synthetic route, in which fine shavings of Ln (Ln = La, Ce, Pr) rod and α-TeO_2 powder were mechanically mixed in a stoichiometric 2:1 ratio in an agate mortar inside a drybox with circulating ultrahigh-purity N_2. The fine shavings of each Ln were obtained by filing the as-purchased rods. The mixtures were placed in graphite crucibles and loaded in a fused-silica ampule. Ampules were subsequently flame-sealed under vacuum at 4.0×10^{-2} Torr and placed centrally inside a muffle furnace. The furnace was heated to 750 °C at a rate of 90 °C/h, where it dwelled for 48 h, and then the furnace was turned off and allowed to come to room temperature for a total of ∼3 days. Additional details on the optimization of this method can be found in the Supporting Information. Products were visibly dark gray-green for Ln = La and Pr and red-brown for Ln = Ce, as seen in Figure 2a−c. Typical yields based on mass were ∼97%, with the small loss of material resulting from multiple transfers.

The tube furnace method employed controlled gas flow through a one-zone horizontal alumina tube equipped with water-chilled endcaps on both ends of the tube and gas outlet vented into a hood. Approximately 1 g of La_2O_3, CeO_2, or Pr_2O_3 was loaded into an alumina boat and spread evenly to ensure maximum exposure to the gas flow. The boat was then placed centrally inside the tube furnace. A separate alumina boat was charged with 15% excess Te shot and placed adjacent to the rare-earth oxide boat on the gas inlet side of the tube furnace (Figure S1). H_2 gas was flowed through the tube furnace at a rate of 30 L/h for 30 min prior to heating to ensure a controlled atmosphere. The furnace was then heated at a rate of 338 °C/h to 700 °C, where it dwelled for 5 h, and then the furnace was turned off and allowed to come to room temperature. The discrepancy in the reaction temperatures between the muffle and tube furnace methods can be attributed to the differences in the diffusion rates. Once the furnace was cooled, H_2 gas flow was stopped, and the furnace was kept closed overnight to continue venting any residual H_2 into the hood. After the sample was removed, excess tellurium that had recrystallized at the cool end of the tube could be mechanically removed. ***Warning!****Elemental Te is considered hazardous with acute inhalation toxicity, and therefore removal from the tube interior must be performed so as not to create dust and should be performed inside a fume hood.* Samples were visibly dark gray-green for Ln = La and Pr and red-brown for Ln = Ce, similar in color to those prepared by the muffle furnace method. Typical yields based on mass were ∼99%.

Ln_2TeO_6 Tellurate Synthesis. Bulk samples of Ln_2TeO_6 (Ln = La, Pr) were prepared by a standard solid-state reaction in a fashion similar to that in a previous report.[16] La_2O_3 and Pr_2O_3 were first calcined in air at 900 °C for 12 h. Ln_2O_3 (Ln = La, Pr) and α-TeO_2 powder were ground in a 1:1 molar ratio using an agate mortar and pestle. The mixture was loaded into an alumina boat and placed centrally inside a muffle furnace. The sample was heated in air at a rate of 75 °C/h to 900 °C, where it dwelled for 36 h, and the furnace was subsequently turned off and allowed to come to room temperature for a total of ∼2.5 days. Samples were visibly white for La_2TeO_6 and pale green for Pr_2TeO_6, as seen in Figure 5a,b. Typical yields based on mass were ∼98%.

Powder X-ray Diffraction (PXRD). For all samples, PXRD data were collected using a PANalytical Empyrean diffractometer with Bragg−Brentano geometry and Ni-filtered Cu Kα radiation (λ = 1.54060 Å) operated at 45 kV voltage and 40 mA current. Data were collected at room temperature over an angular range of $10° \leq 2\theta \leq 90°$ at a scan rate of 0.04°/min and a step width of 0.008°. The *X'Pert Plus* software package was utilized for X-ray diffraction (XRD) data analysis, and a previously established structural model was used for Rietveld refinement. Global profile refinement parameters included a scale factor, a specimen displacement parameter, and a peak shape function (U, V, and W, respectively) using the Caglioti equation. The peak shape was fit using a pseudo-Voigt function, and the background was manually determined. The unit cell parameters, site occupancies, and isotropic displacement parameters were refined. The PXRD patterns for Ln_2O_2Te (Ln = La, Ce, Pr) and Ln_2TeO_6 (Ln = La, Pr) are shown in Figures S2−S6.

Diffuse-Reflectance Spectroscopy (DRS). The optical band gaps of all synthesized bulk samples were determined by DRS measurements and Tauc analyses. DRS data were collected from 200 to 1100 nm using a PerkinElmer Lambda 365 spectrophotometer equipped with an integrating-sphere accessory. The reflectance data was converted to absorbance data via the Kubelka−Munk equation $\alpha/S = (1 - R)^2/2R$, where α is the absorption coefficient, S is the scattering factor, and R is the reflectance at a given wavelength.[17] Tauc plots are based on the equation $h\nu = \alpha(h\nu - E_g)^n$, where E_g represents the energy band gap and n denotes the mode of electronic transition, i.e., $n = {}^1/_2$ for a direct transition and $n = 2$ for an indirect transition.[17,18]

Differential Scanning Calorimetry (DSC) and Thermogravimetric Analysis (TGA). The thermal stability was determined by DSC/TGA using a TA Instruments SDT650 analyzer. A total of 10 mg of each sample was loaded into an alumina crucible and heated to 1000 °C at 20 °C/min under a constant 50 mL/min air flow.

Electron Microscopy. Measurements were performed by scanning electron microscopy (Hitachi S-3000N) in conjuction with energy-dispersive X-ray spectrophotometry (EDS). EDS scans were collected at an accelerating voltage of 30 kV, a current at 50 mA, and 2K× magnification. EDS was used for elemental analysis, and scans were collected between 0 and 10 keV.

■ RESULTS AND DISCUSSION

Synthesis of Ln_2O_2Te Oxytelluride in a Tube Furnace. According to a previous report,[19] the Ln_2O_2Te synthesis can be described by eq 1, where H_2 serves as a carrier gas to sweep Te vapor over Ln_2O_3 (or CeO_2).

$$Ln_2O_3(s) + Te(g) + H_2(g) \rightarrow Ln_2O_2Te(s) + H_2O(g) \quad (1)$$

In the case of Ce_2O_2Te,

$$2CeO_2(s) + Te(g) + 2H_2(g) \rightarrow Ce_2O_2Te(s) + 2H_2O(g) \quad (2)$$

To test this, we attempted this same synthesis using N_2 or Ar gas in place of H_2. Formation of the Ln_2O_2Te product was not successful with N_2 or Ar gas flow. Rather, unreacted Ln_2O_3 (or CeO_2) remained in the reaction boat. Furthermore, Te metal was not deposited at the cool zone of the furnace, which suggests that H_2 serves as a reducing agent (to reduce Te^0 to Te^{2-}) and is not simply a carrier gas. The role of hydrogen in this reaction will be the focus of future studies.

Crystal Structure of Ln_2O_2Te Oxytelluride. The oxytelluride Ln_2O_2Te (Ln = La, Ce, Pr) crystallizes in the

https://doi.org/10.1021/acs.inorgchem.2c02287
Inorg. Chem. 2022, 61, 18002−18009

tetragonal *anti*-$ThCr_2Si_2$ structure type, *I*4/*mmm* (No. 139) shown in Figure 1a. Crystallographic results obtained from

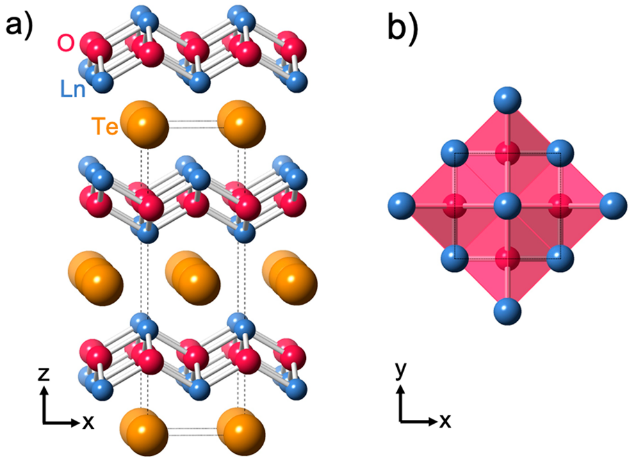

Figure 1. (a) Crystal structure of Ln_2O_2Te (Ln = La, Ce, Pr) with alternating $[Ln_2O_2]^{2+}$ and Te^{2-} layers along [001]. (b) View of the edge-sharing OLn_4 tetrahedra along [001].

Rietveld refinements are summarized in Tables S1 and S2. In this structure, the anions segregate into alternating $[Ln_2O_2]^{2+}$ and Te^{2-} layers. Puckered two-dimensional $[Ln_2O_2]^{2+}$ layers contain fluorite-like OLn_4 tetrahedra, a common structural feature among oxychalcogenides,[9,20] with edge-sharing connectivity (Figure 1b), and these are related by an *ab* mirror plane along [001]. The symmetry of the $[Ln_2O_2]^{2+}$ layers in Ln_2O_2Te differs from that of Ln_2O_2Q (Q = S, Se), where $[Ln_2O_2]^{2+}$ layers are simply translated along [001] (with no mirror plane).[9] The larger interlayer spacing of ∼4.14 Å in Ln_2O_2Te, compared to ∼3.89−4.11 Å in Ln_2O_2Q (Q = S, Se), can accommodate larger Te^{2-} anions. The Te^{2-} layer is characterized by square nets of Te atoms, a distinctive structural motif in polytelluride compounds.[21] The Te−Te distances of ∼4.1 Å are much larger than those of other square-net-containing polytellurides (2.8−3.4 Å) but still within the van der Waals contact distance (4.2 Å), indicating weak Te−Te interactions.[22] Each Te^{2-} anion is coordinated by 8 Ln atoms with a Te−Ln distance of ∼3.6 Å (Table S3), which is expected for a 2− oxidation state for Te according to bond valence models.[23] The Ln^{3+} site is coordinated by eight atoms (4O + 4Te) in a distorted square antiprism with Ln−O distances of ∼2.4 Å, similar to the Ln−O distances in other heteroanionic systems.[24,25]

Optical Properties of Ln_2O_2Te Oxytelluride. The DRS spectra of the as-prepared Ln_2O_2Te (Ln = La, Ce, Pr) are shown in Figure 2. Tauc plots display optical transitions, as shown in the inset of Figure 2, and were used to estimate the energy band gaps. The large drop in reflectance with decreasing wavelength corresponds to the valence → conduction band absorption edge. The band-gap values for La_2O_2Te, Ce_2O_2Te, and Pr_2O_2Te were determined to be E_g = 2.7, 2.1, and 2.6 eV, respectively, consistent with calculated values of indirect optical transitions (taking into account that the calculated band gaps tend to be underestimated).[26] The results for La_2O_2Te also agree with a previously reported DRS measurement.[27] For Pr_2O_2Te, small absorption peaks in the 450−600 nm range (marked by asterisks) result from characteristic intra-4*f* electronic transitions of Pr^{3+}.

Ln_2O_2Te Oxytelluride to Ln_2TeO_6 Tellurate Phase Transition. Each Ln_2O_2Te (Ln = La, Ce, Pr) sample was subjected to thermal analysis and TGA under an air flow. The resulting DSC/TGA first heating curves are shown in Figure 3, with thermal events labeled numerically. Surprisingly, each rare-earth oxytelluride analogue has a unique thermal curve.

For La_2O_2Te, the first two exothermic peaks centered at 400 and 540 °C in Figure 3a are collectively associated with a 9% weight gain due to oxidation and suggest possible metastable phases, such as the hypothetical La_2TeO_5 stoichiometry speculated by Kent and Eick.[19] Peaks 1 and 2 could not be resolved using slower heating rates without significantly reducing the DSC sensitivity, and our initial attempts to quench the crystalline samples at these temperatures were unsuccessful. Investigations into possible metastable phases are underway. A glass transition is observed at the endothermic peak 3 with an onset of 750 °C, indicating an amorphous transition. Finally, an additional small weight gain linked to the

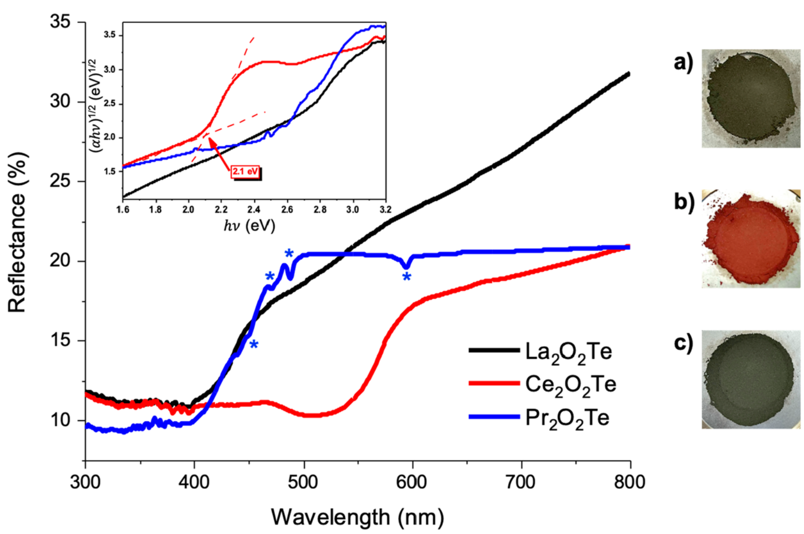

Figure 2. DRS spectra and Tauc plots (inset) for Ln_2O_2Te (Ln = La, Ce, Pr). Photographs of (a) La_2O_2Te, (b) Ce_2O_2Te, and (c) Pr_2O_2Te on the right show color variations.

https://doi.org/10.1021/acs.inorgchem.2c02287
Inorg. Chem. 2022, 61, 18002−18009

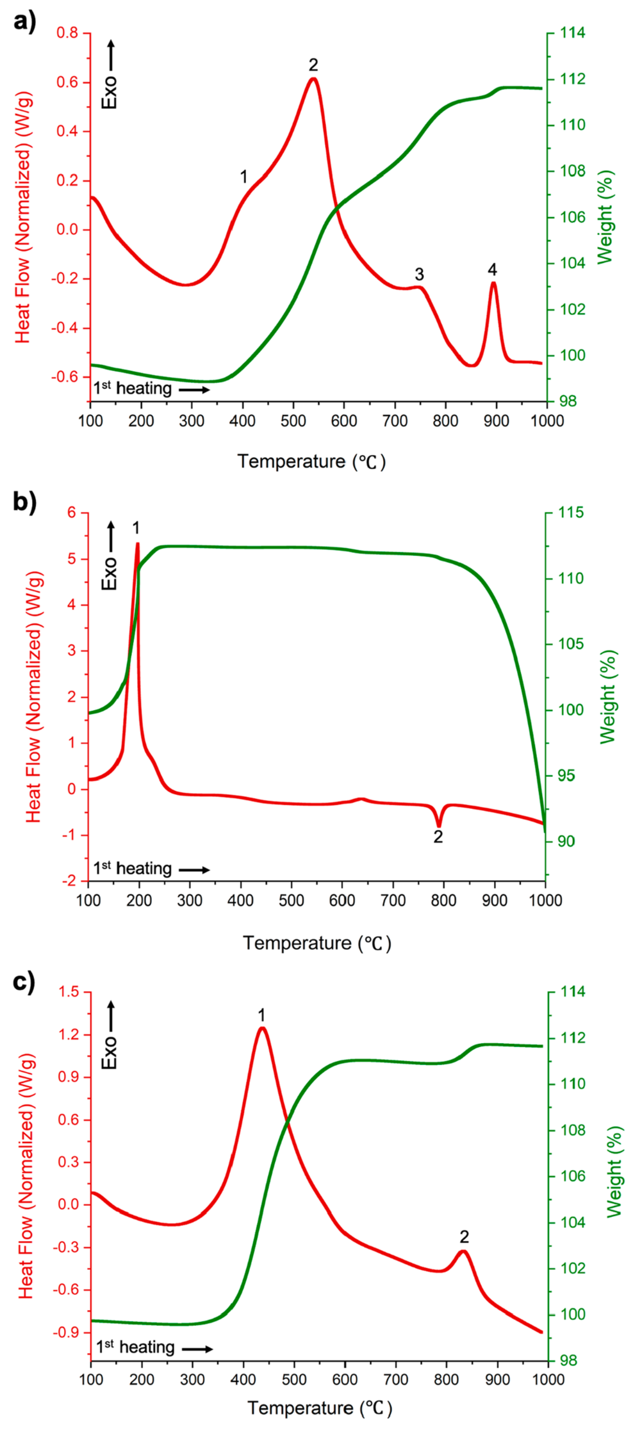

Figure 3. DSC (red) and TGA (green) curves for (a) La_2O_2Te, (b) Ce_2O_2Te, and (c) Pr_2O_2Te.

exothermic peak 4 centered at 900 °C is related to the crystallization of La_2TeO_6. This composition was confirmed by XRD (Figure 4) and indicates a stepwise temperature-dependent oxytelluride-to-tellurate phase transition with increasing temperature in air. Bi_2O_2Te, which is isostructural with La_2O_2Te, also exhibits an oxytelluride to Bi_2TeO_6 tellurate phase transition upon heating in air.[28,29] In Bi_2TeO_6, Te^{6+} is octahedrally coordinated with O.[28,30]

Pr_2O_2Te shows a similar oxytelluride-to-tellurate phase transition, as seen in Figure 3c, but only two major thermal events linked to weight change are observed. The exothermic peak 1 centered at 440 °C is associated with an 11% weight gain due to oxidation and also suggests a metastable phase with Pr_2TeO_5 stoichiometry. The exothermic peak 2 centered at 835 °C is accompanied by a small weight gain and indicates the crystallization of Pr_2TeO_6, which was confirmed by XRD (Figure S7).

To further investigate the oxytelluride-to-tellurate phase transition, Ln_2TeO_6 (Ln = La, Pr) samples were prepared directly from metal oxides, as described in the Experimental Section. Heating Ln_2TeO_6 (Ln = La, Pr) to 700 °C under a H_2 gas flow results in a phase transition back to Ln_2O_2Te (Ln = La, Pr), as identified by XRD in Figures 4 and S7. Thus, the transition between the Ln_2O_2Te and Ln_2TeO_6 phases is reversible by warming in the appropriate oxidizing/reducing atmosphere. To the best of our knowledge, this phase reversibility is not reported for other chalcogen analogues and showcases the versatility of tellurium.

Crystal Structure of Ln_2TeO_6 Tellurate. Ln_2TeO_6 (Ln = La, Pr) tellurate crystallizes in the orthorhombic structure type and $P2_12_12_1$ (No. 19) space group. The crystallographic results obtained from Rietveld refinements are summarized in Tables S1 and S2. The tellurate structure, displayed in Figure 5a, differs from the oxytelluride structure primarily in the cationic role of Te. In this structure, Te is octahedrally coordinated with O and can be assigned the 6+ oxidation state. Although chalcogenides are known for their broad range of oxidation states, from 2− to 6+, these Te-centered octahedra (Figure 5b) are unique to tellurates. By contrast, sulfates and selenates are commonly characterized by tetrahedral coordination of chalcogen, which bonds more tightly with the O atoms.[14]

Unlike the layered oxytelluride, the tellurate structure is three-dimensional and constructed from distorted TeO_6 octahedra and LnO_7 polyhedra. Bond distances and bond angles for the TeO_6 octahedra and LnO_7 (Ln = La, Pr) polyhedra are listed in Tables S3 and S4. The TeO_6 octahedra are trigonally distorted from idealized octahedral symmetry, as seen in Figure 5b. The Te−O distances range between 1.84 and 2.03 Å, comparable to those of other tellurate compounds with Te^{6+}-to-O^{2-} distances (1.83−1.95 Å).[31,32] A bond valence analysis using local interatomic distances is presented in Table S5. The bond valences around Te sum to 6.23 and 5.82 in La_2TeO_6 and Pr_2TeO_6, respectively, close to a 6+ oxidation state. The slight over or under bonding for Te is compensated for by the two rare-earth sites Ln1 and Ln2. The O−Te−O bond angles (Table S4) also demonstrate deviations from ideal octahedral symmetry and range from 80.2 to 100.1°. Each TeO_6 octahedron is surrounded by a total of nine LnO_7 polyhedra, so that TeO_6 octahedra are completely isolated from each other, thereby distinguishing the rare-earth Ln_2TeO_6 tellurate from Bi_2TeO_6. Three of the nine LnO_7 polyhedra share an edge with the TeO_6 octahedron through O2−O5, O2−O6, and O3−O5 pairs, and the remaining six LnO_7 polyhedra share a corner with the octahedron. The coordination around the two rare-earth sites is shown in Figure 5c. $Ln1O_7$ and $Ln2O_7$ polyhedra share an edge through O1−O5. The Ln−O interatomic distances in the LnO_7 polyhedra range between 2.23 and 2.69 Å and reflect distances in the LnO_7 polyhedra of Ln_2O_3 rare-earth sesquioxides.[33]

Optical Properties of Ln_2TeO_6 Tellurate. The DRS spectra of the Ln_2TeO_6 (Ln = La, Pr) samples are shown in Figure 6, and Tauc plots are displayed in the inset. The energy-band-gap values for La_2TeO_6 and Pr_2TeO_6 were determined to

https://doi.org/10.1021/acs.inorgchem.2c02287
Inorg. Chem. 2022, 61, 18002−18009

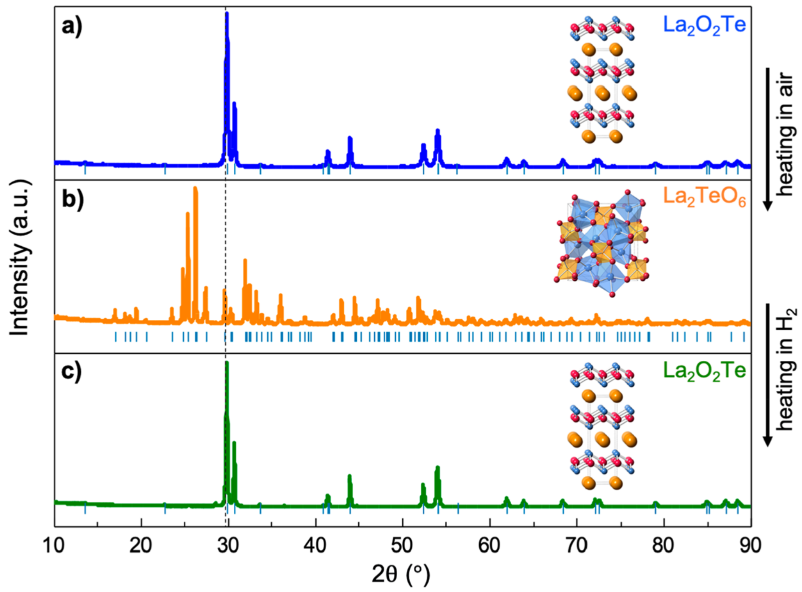

Figure 4. PXRD patterns demonstrating the oxytelluride-to-tellurate phase transition of samples, in which (a) La_2O_2Te synthesized by the tube furnace method was heated in air to form (b) La_2TeO_6, which was then heated in H_2 to form (c) La_2O_2Te. Tick marks show Bragg reflections, and a dashed line has been added as a guide for the eye.

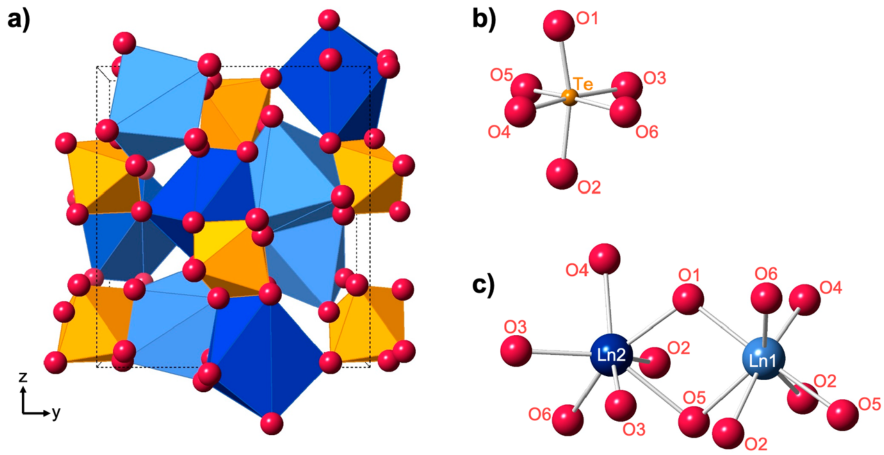

Figure 5. (a) Crystal structure and unit cell of Ln_2TeO_6 (Ln = La, Pr). Local environments of (b) a distorted TeO_6 octahedron and (c) a LnO_7 polyhedron.

be 4.3 and 3.7 eV, respectively. For Pr_2TeO_6, the characteristic intra-4*f* electronic transitions of Pr^{3+} are more clearly seen due to Stark splitting. According to the energy-level diagram proposed by Dieke and Crosswhite,[34] the group of absorption bands located at 448, 477, and 490 nm can be assigned to $^3H_4 \rightarrow {}^3P_J$ (J = 2, 1, 0) transitions. The peak at 600 nm can be assigned to the $^3H_4 \rightarrow {}^1D_2$ transition.

Decomposition of Ce_2O_2Te Oxytelluride. The stability of Ce_2O_2Te is markedly different from those of La_2O_2Te and Pr_2O_2Te, as seen in Figure 3b. The exothermic peak 1 centered at 200 °C is associated with a ∼12% weight gain, indicating oxidation corresponding to $\sim Ce_2O_{5.3}Te$ stoichiometry; however, we were not able to experimentally isolate this phase. In contrast with the La_2O_2Te and Pr_2O_2Te samples, a large 23% weight loss linked with the endothermic peak 2 centered at 790 °C denotes melting. XRD and EDS analyses confirmed the presence of CeO_2 in post-TGA samples; absorption edges associated with tellurium were not observed in the EDS spectra (Figures S8 and S9).

To probe the instability of Ce_2O_2Te, a timelapse experiment was conducted in which a single sample synthesized by the muffle furnace method was monitored by XRD and DRS in ambient conditions over the course of 1 year. A timelapse of the XRD patterns (Figure 7) shows that the most intense peaks for Ce_2O_2Te at $2\theta = 30.2°$ and 31.0° gradually decrease in intensity, concurrent with the peaks corresponding to $CeO_{1.996}$ (PDF 01-075-7751) and $CeO_{1.695}$ (PDF 01-089-8429) increasing as the sample ages. Furthermore, a timelapse of the reflectance data (Figure 8) show the emergence and growth of a secondary peak at 465 nm, which is in agreement with the optical properties previously reported for CeO_2.[35,36] We also observed that the sample color faded from dark red to light red-brown over the course of 1 year.

■ CONCLUSION

The outstanding versatility of Te in terms of its structure, properties, and reactivity is showcased in the oxytelluride and

https://doi.org/10.1021/acs.inorgchem.2c02287
Inorg. Chem. 2022, 61, 18002−18009

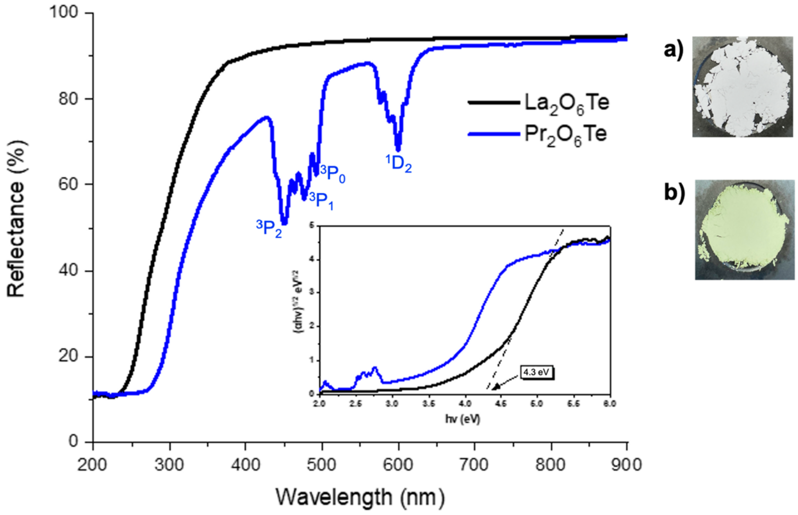

Figure 6. DRS spectra and Tauc plots (inset) for Ln_2TeO_6 (Ln = La, Pr) and photographs of (a) La_2TeO_6 and (b) Pr_2TeO_6.

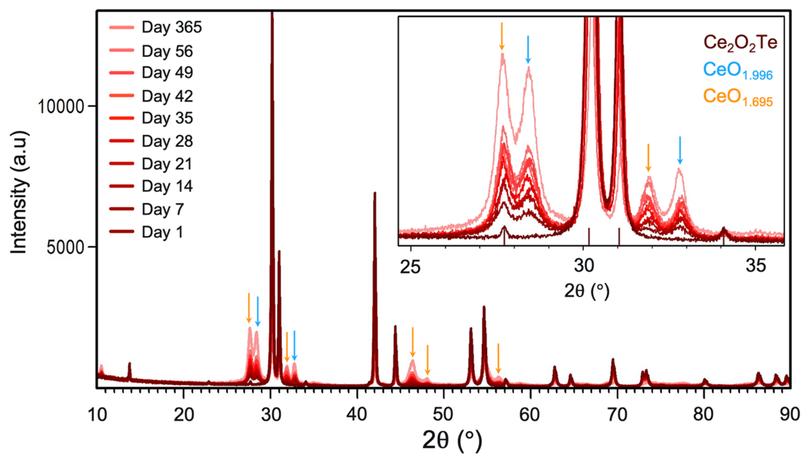

Figure 7. Timelapse XRD pattern of Ce_2O_2Te. Inset: Zoomed image of peaks in the 2θ range 25−35°, where phases are denoted with color-coordinated arrows and tick marks.

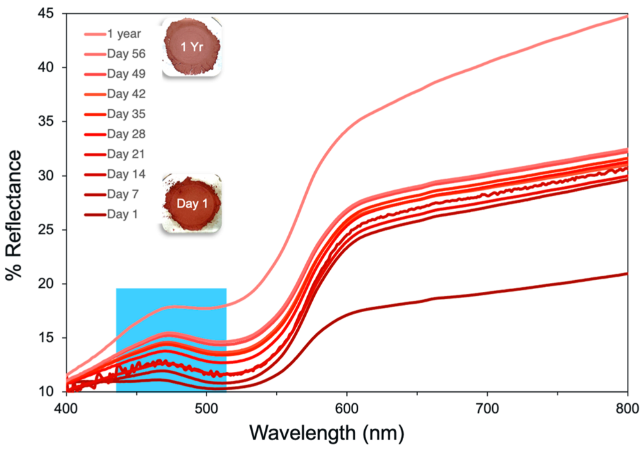

Figure 8. Timelapse DRS spectra of Ce_2O_2Te. The blue highlighted region emphasizes the gradual emergence and growth of a secondary peak. Photographs of the sample show the color change over time.

tellurate phases presented here. Ln_2O_2Te (Ln = La, Ce, Pr) was synthesized by a standard solid-state method, wherein Te is reduced from 4+ to 2− oxidation state, and by a H_2 gas flow, wherein Te is reduced from 0 to 2− oxidation state. Heating the oxytelluride in air to temperatures above 850 °C results in a stepwise phase transition to tellurate Ln_2TeO_6 (Ln = La, Pr), in which Te is oxidized to 6+, with the exception of Ce_2O_2Te, which proved to be unstable and degraded to CeO_2. The synthetic conditions detailed here demonstrate that the broad range of the Te oxidation states from 2− to 6+ can be accessed by heating in the appropriate reducing/oxidizing atmosphere and, if exploited creatively, may facilitate an expansion of Te-containing compounds. The optical properties for Ln_2O_2Te (Ln = La, Ce, Pr), which fall in the semiconducting range, and for Ln_2TeO_6 (Ln = La, Pr) are presented here for the first time. We anticipate that the reversibility of an oxytelluride-to-tellurate phase transition, which has not been observed for lighter oxychalcogenide analogues, could advance materials science research with regard to tellurium chemistry and band-gap control via reductive/oxidative reactions.

■ ASSOCIATED CONTENT

Supporting Information

The Supporting Information is available free of charge at https://pubs.acs.org/doi/10.1021/acs.inorgchem.2c02287.

https://doi.org/10.1021/acs.inorgchem.2c02287
Inorg. Chem. 2022, 61, 18002−18009

Additional synthetic details, PXRD patterns of Ln_2O_2Te (Ln = La, Ce, Pr) and Ln_2TeO_6 (Ln = La, Pr), crystallographic and structure refinement data of Ln_2O_2Te (Ln = La, Ce, Pr) and Ln_2TeO_6 (Ln = La, Pr), selected bond distances and bond angles for Ln_2O_2Te (Ln = La, Ce, Pr) and Ln_2TeO_6 (Ln = La, Pr), bond valence sums for Ln_2TeO_6 (Ln = La, Pr), PXRD pattern of the Ce_2O_2Te sample after 1 year, PXRD data of CeO_2, EDS spectrum of the Ce_2O_2Te sample after heating to 1000 °C (PDF)

■ AUTHOR INFORMATION

Corresponding Author

Robin T. Macaluso − *Department of Chemistry and Biochemistry, University of Texas at Arlington, Arlington, Texas 76019, United States;* orcid.org/0000-0002-0021-0775; Email: robin.macaluso@uta.edu

Authors

Melissa S. Orr − *Department of Chemistry and Biochemistry, University of Texas at Arlington, Arlington, Texas 76019, United States*

Katheryn R. Cruz − *Department of Chemistry and Biochemistry, University of Texas at Arlington, Arlington, Texas 76019, United States*

Hoa H. Nguyen − *Department of Chemistry and Biochemistry, University of Texas at Arlington, Arlington, Texas 76019, United States;* orcid.org/0000-0002-3375-4998

Akari L. Kojima − *Department of Chemistry and Biochemistry, University of Texas at Arlington, Arlington, Texas 76019, United States*

Complete contact information is available at: https://pubs.acs.org/10.1021/acs.inorgchem.2c02287

Notes

The authors declare no competing financial interest.

■ ACKNOWLEDGMENTS

This material is based upon work supported by the National Science Foundation under Grants GRFP 2136537 and DMR 2113689. Any opinions, findings, and conclusions or recommendations expressed in this material are those of the authors and do not necessarily reflect the views of the National Science Foundation.

■ REFERENCES

(1) Kageyama, H.; Hayashi, K.; Maeda, K.; Attfield, J. P.; Hiroi, Z.; Rondinelli, J. M.; Poeppelmeier, K. R. Expanding Frontiers in Materials Chemistry and Physics with Multiple Anions. *Nat. Commun.* **2018**, *9* (1), 772.

(2) Valldor, M. Anion Ordering in Bichalcogenides. *Inorganics* **2016**, *4* (3), 23.

(3) Tripathi, T. S.; Karppinen, M. Mixed-Anion Compounds: An Unexplored Playground for ALD Fabrication. *Advanced Materials Interfaces* **2021**, *8* (11), 2100146.

(4) Li, Y.; Singh, D. J. First Principles Based Screen for Identification of Transparent Conductors. *Journal of Materials Chemistry C* **2019**, *7* (8), 2436−2442.

(5) Williamson, B. A. D.; Limburn, G. J.; Watson, G. W.; Hyett, G.; Scanlon, D. O. Computationally Driven Discovery of Layered Quinary Oxychalcogenides: Potential p-Type Transparent Conductors? *Matter* **2020**, *3* (3), 759−781.

(6) Yim, K.; Youn, Y.; Lee, M.; Yoo, D.; Lee, J.; Cho, S. H.; Han, S. Computational Discovery of p-type Transparent Oxide Semiconductors Using Hydrogen Descriptor. *npj Computational Materials* **2018**, *4* (1), 17.

(7) He, J.; Yao, Z.; Hegde, V. I.; Naghavi, S. S.; Shen, J.; Bushick, K. M.; Wolverton, C. Computational Discovery of Stable Heteroanionic Oxychalcogenides ABXO (A, B = Metals; X = S, Se, and Te) and Their Potential Applications. *Chem. Mater.* **2020**, *32* (19), 8229−8242.

(8) Zhao, X.; Zhao-Karger, Z.; Wang, D.; Fichtner, M. Metal Oxychlorides as Cathode Materials for Chloride Ion Batteries. *Angew. Chem.* **2013**, *125* (51), 13866−13869.

(9) Orr, M.; Hebberd, G. R.; McCabe, E. E.; Macaluso, R. T. Structural Diversity of Rare-Earth Oxychalcogenides. *ACS Omega* **2022**, *7* (10), 8209−8218.

(10) Larquet, C.; Carenco, S. Metal Oxysulfides: From Bulk Compounds to Nanomaterials. *Frontiers in Chemistry* **2020**, *8*, 179.

(11) Ahmed, M.; Xinxin, G. A Review of Metal Oxynitrides for Photocatalysis. *Inorganic Chemistry Frontiers* **2016**, *3* (5), 578−590.

(12) Chivers, T.; Laitinen, R. S. Tellurium: A Maverick Among the Chalcogens. *Chem. Soc. Rev.* **2015**, *44* (7), 1725−1739.

(13) Hurd, A. J.; Kelley, R. L.; Eggert, R. G.; Lee, M.-H. Energy-Critical Elements for Sustainable Development. *MRS Bull.* **2012**, *37* (4), 405−410.

(14) Cotton, F. A.; Willkinson, F. G.*Advanced Inorganic Chemistry*, 5th ed.; John Wiley and Sons, Inc.: New York, 1988; pp 491−543.

(15) Lee, S. Y.Synthesis and Photochemistry of Hydrogen Telluride. Masters Thesis, University of Southern California, Los Angeles, CA, 2004.

(16) Tang, J.; Gou, J.; Li, G.; He, H.; Li, Y.; Li, C. Tunable Upconversion Luminescence from the Phosphors of Yb^{3+}, Tm^{3+} and Ho^{3+} tri-doped Re_2TeO_6 (Re = La, Gd, and Lu). *J. Alloys Compd.* **2016**, *672*, 1−6.

(17) Murphy, A. B. Band-gap Determination from Diffuse Reflectance Measurements of Semiconductor Films, and Application to Photoelectrochemical Water-Splitting. *Sol. Energy Mater. Sol. Cells* **2007**, *91* (14), 1326−1337.

(18) Viezbicke, B. D.; Patel, S.; Davis, B. E.; Birnie, D. P. Evaluation of the Tauc Method for Optical Absorption Edge Determination: ZnO Thin Films as a Model System. *Physica Status Solidi B* **2015**, *252* (8), 1700−1710.

(19) Kent, R. A.; Eick, H. A. The Preparation and Properties of Some Lanthanum(III) Monotelluroöxides. *Inorg. Chem.* **1962**, *1* (4), 956−958.

(20) Luu, S. D. N.; Vaqueiro, P. Layered Oxychalcogenides: Structural Chemistry and Thermoelectric Properties. *Journal of Materiomics* **2016**, *2* (2), 131−140.

(21) Graf, C.; Assoud, A.; Mayasree, O.; Kleinke, H. Solid State Polyselenides and Polytellurides: A Large Variety of Se−Se and Te−Te Interactions. *Molecules* **2009**, *14* (9), 3115−3131.

(22) Bondi, A. V. van der Waals Volumes and Radii. *J. Phys. Chem.* **1964**, *68* (3), 441−451.

(23) Christy, A. G.; Mills, S. J.; Kampf, A. R. A Review of the Structural Architecture of Tellurium Oxycompounds. *Mineralogical Magazine* **2016**, *80* (3), 415−545.

(24) Ueda, K.; Takafuji, K.; Hosono, H. Preparation and Crystal Structure Analysis of CeCuOS. *J. Solid State Chem.* **2003**, *170* (1), 182−187.

(25) Liu, M. L.; Wu, L. B.; Huang, F. Q.; Chen, L. D.; Ibers, J. A. Syntheses, Crystal and Electronic Structure, and Some Optical and Transport Properties of LnCuOTe (Ln = La, Ce, Nd). *J. Solid State Chem.* **2007**, *180* (1), 62−69.

(26) Mahmood, A.; Ramay, S. M.; Saeed, Y. First Principles Study of Band Structure and Density of States of Rare Earth Oxytellurides R_2O_2Te (R = La, Ce, Pr, and Nd). *Optoelectronics and Advanced Materials - Rapid Communications* **2014**, *8* (7−8), 724−726.

(27) Llanos, J.; Conejeros, S.; Cortés, R.; Sánchez, V.; Barahona, P.; Peña, O. Optical, Magnetic and Electronic Properties of Ln_2O_2Te (Ln = La, Sm and Gd). *Mater. Res. Bull.* **2008**, *43* (2), 312−319.

(28) Luu, S. D. N.; Vaqueiro, P. Synthesis, Characterisation and Thermoelectric Properties of the Oxytelluride Bi_2O_2Te. *J. Solid State Chem.* **2015**, *226*, 219−223.
(29) Udovic, M.; Valant, M.; Suvorov, D. Formation and Decomposition of the Bi_2TeO_6 Compound. *Journal of the European Ceramic Society* **2004**, *24* (6), 953−958.
(30) Schmidt, P.; Bosholm, O.; Oppermann, H. Investigations of the Ternary System Bi/Te/O, II. The Thermal Behaviour and the Relations of Phase Coexistences of Bi_2O_2Te. *Zeitschrift für Naturforschung B* **1997**, *52* (12), 1461−1466.
(31) Sullens, T. A.; Albrecht-Schmitt, T. E. Structure and Properties of the Thorium Vanadyl Tellurate, $Th(VO_2)_2(TeO_6)(H_2O)_2$. *Inorg. Chem.* **2005**, *44* (7), 2282−2286.
(32) Wang, D.; Zhang, Y.; Liu, Q.; Zhang, B.; Yang, D.; Wang, Y. Band Gap Modulation and Nonlinear Optical Properties of Quaternary Tellurates Li_2GeTeO_6. *Dalton Trans.* **2022**, *51* (23), 8955−8959.
(33) Pauling, L. The Crystal Structure of the A-Modification of the Rare Earth Sesquioxides. *Zeitschrift für Kristallographie - Crystalline Materials* **1929**, *69* (1−6), 415−421.
(34) Dieke, G. H.; Crosswhite, H. M. The Spectra of the Doubly and Triply Ionized Rare Earths. *Appl. Opt.* **1963**, *2* (7), 675−686.
(35) Kitsou, I.; Arkas, M.; Tsetsekou, A. Synthesis and Characterization of Ceria-Coated Silica Nanospheres: Their Application in Heterogeneous Catalysis of Organic Pollutants. *SN Applied Sciences* **2019**, *1* (12), 1−12.
(36) Fiorenza, R.; Bellardita, M.; D'Urso, L.; Compagnini, G.; Palmisano, L.; Scirè, S. Au/TiO_2-CeO_2 Catalysts for Photocatalytic Water Splitting and VOCs Oxidation Reactions. *Catalysts* **2016**, *6* (8), 121.

https://doi.org/10.1021/acs.inorgchem.2c02287
Inorg. Chem. 2022, 61, 18002−18009